

Dark matter annihilation effects on the first stars

F. Iocco¹, A. Bressan^{2,3,4}, E. Ripamonti⁵, R. Schneider¹, A. Ferrara⁴, P. Marigo⁶

¹INAF/Osservatorio Astrofisico di Arcetri; Largo Enrico Fermi 5, Firenze, Italy

²INAF/Osservatorio Astronomico di Padova; Vicolo dell’Osservatorio 5, Padova, Italy

³INAOE; Luis Enrique Erro 1, 72840, Tonantzintla, Puebla, Mexico

⁴SISSA; Via Beirut 4, Trieste, Italy

⁵Università degli Studi dell’Insubria, Dip. di Scienze Chimiche, Fisiche e Naturali; Via Valleggio 12, Como, Italy

⁶Università degli Studi di Padova, Dip. di Astronomia; Vicolo dell’Osservatorio 3, Padova, Italy

30 October 2018

ABSTRACT

We study the effects of weakly interacting massive particles (WIMP) dark matter (DM) on the collapse and evolution of the first stars in the Universe. Using a stellar evolution code, we follow the pre-Main Sequence (MS) phase of a grid of metal-free stars with masses in the range $5M_{\odot} \leq M_{*} \leq 600M_{\odot}$ forming in the centre of a 10^6M_{\odot} halo at $z = 20$. DM particles of the parent halo are accreted in the proto-stellar interior by adiabatic contraction and scattering/capture processes, reaching central densities of $\mathcal{O}(10^{12} \text{ GeV cm}^{-3})$ at radii of the order of 10 AU. Energy release from annihilation reactions can effectively counteract the gravitational collapse, in agreement with results from other groups. We find this stalling phase (known as a *dark star*) is transient and lasts from $2.1 \times 10^3 \text{ yr}$ ($M_{*} = 600M_{\odot}$) to $1.8 \times 10^4 \text{ yr}$ ($M_{*} = 9M_{\odot}$). Later in the evolution, DM scattering/capture rate becomes high enough that energy deposition from annihilations significantly alters the pre-MS evolution of the star in a way that depends on DM (i) velocity dispersion, \bar{v} , (ii) density, ρ , (iii) elastic scattering cross section with baryons, σ_0 . For our fiducial set of parameters $(\bar{v}, \rho, \sigma_0) = (10 \text{ km s}^{-1}, 10^{11} \text{ GeV cm}^{-3}, 10^{-38} \text{ cm}^2)$ we find that the evolution of stars of mass $M_{*} < 40M_{\odot}$ “freezes” on the HR diagram before reaching the ZAMS. Stars with $M_{*} \geq 40M_{\odot}$ manage to ignite nuclear reactions; however, DM “burning” prolongs their lifetimes by a factor 2 (5) for a $600M_{\odot}$ ($40M_{\odot}$) star.

Key words: early universe– stellar formation–dark matter

1 INTRODUCTION

Current observations of primordial light element abundances, baryon acoustic oscillations, distance measurements by means of Type Ia supernovae and cosmic microwave background, all fit together to describe a Universe undergoing an accelerated expansion (see Spergel et al. 2007; Komatsu et al. 2008 and references therein). An unknown energy field, often referred to as Dark Energy, constitutes approximately 75% of the total energy density, whereas the remaining is made of matter. However, only 15% of the latter is made of known particles (baryons): its majority seems to be composed of a non-visible, unknown component, commonly referred to as Dark Matter (DM). If thermally produced in the hot plasma, models best fitting observations require it to have decoupled at temperatures much smaller than its mass, thus being often referred to as *cold*.

In this scenario, small scale perturbations grow faster and detach first from the Hubble flow, leading to a “hierarchical” growth of structures starting off very small haloes in the young universe, and building up bigger ones by means of

mergers. The first stars are predicted to form at $z < 20 - 30$ in haloes with masses $M = 10^6 - 10^8 M_{\odot}$, generally referred to as mini-haloes (see Barkana & Loeb 2001 and Ciardi & Ferrara 2005 for thorough reviews of the subject). The gas virialized in the potential wells of these systems has primordial chemical composition and low temperatures, $T_{\text{vir}} < 10^4 \text{ K}$; in these conditions the additional cooling necessary for the gas to collapse and form stars is provided by molecular hydrogen. The results of recent semi-analytic studies and of sophisticated 3D numerical simulations consistently indicate that the reduced cooling efficiency, together with the absence of magnetic fields and of relevant angular momentum effects, inhibits gas fragmentation and lead to the formation of a single massive star (Omukai & Nishi 1998; Bromm, Coppi & Larson 1999, 2001; Abel et al. 2000, 2002; Nakamura & Umemura 2001; Ripamonti et al. 2002; Gao et al. 2007; O’Shea & Norman 2007; Yoshida et al. 2006, 2007). The mass of these first stars, often called Population III (Pop III) stars, is still uncertain but likely to be in the range $30M_{\odot} < M_{*} < 300M_{\odot}$, depending on the

strength of feedback effects which control the mass growth by accretion on the central high-density core (Omukai & Palla 2003; Tan & McKee 2004).

Since Pop III stars are predicted to form at high z or are hidden in the outskirts of collapsing structures at moderate z (Schneider et al. 2006; Tornatore, Schneider & Ferrara 2007), observational evidences of their nature and properties are still lacking. If very massive, they are thought to explode as powerful pair-instability supernovae or to directly collapse to black holes after a short lifetime of a few Myr (Heger & Woosley 2002). The chemical imprint they leave on subsequent stellar generations is difficult to identify in current samples of extremely metal-poor stars in the Galactic halo (Tumlinson 2006; Salvadori, Schneider & Ferrara 2007); their signature on the reionization history is weak (Gnedin & Fan 2006; Choudhury & Ferrara 2006), and so is any feature in the low and high energy diffuse neutrino background (Schneider, Guetta & Ferrara 2001; Iocco et al. 2005, 2008). Future probes of the nature of Pop III stars will come from the James Webb Space Telescope or from 21cm telescopes which are expected to operate within the next decade.

Intricate as the “standard” scenario can be, with ordinary matter only gravitationally interacting with its dark counterpart, there are instances where the situation could have been complicated by additional interactions between dark and ordinary matter.

There is a flourishing zoology of models providing candidates for DM particles, and we address the reader to Bertone, Hooper & Silk (2005) for a thorough review of motivations, candidates, and their properties. The currently favored model, which naturally complies with the requirements arising from cosmological and particle physics arguments, is the lightest stable particle in a supersymmetric extension of the standard model of particle physics. Often referred to as *neutralinos*, these are Majorana particles coupled to baryons by means of weak interactions, with the most remarkable properties to be self-annihilating, and to have a non-vanishing scattering cross-section with standard model particles.

For what concerns this paper, the consequence of these properties is two-fold: in environments with high enough density of DM particles, self-annihilation of neutralinos could constitute a source of energy, emitted in the form of radiation, which can potentially overcome the cooling of the gas, inhibiting or slowing down the formation of a proto-star. When (and if) something resembling a celestial object is formed, such weakly interacting massive particles (WIMPs) can scatter off the baryonic material and lose energy, thus being gravitationally captured; they accumulate and annihilate inside the object, thus providing it with an (additional) energy source.

At present, the typical DM densities are too low to provide any dramatic, widespread effect on stellar evolution: recent calculations show that DM densities necessary to induce strong effects are achievable only within the central two parsecs of our galaxy, with similar restrictions applying to all galaxies in the Local Universe (Fairbairn, Scott & Edsjo, 2008). The first star-forming mini-haloes, however, are smaller and denser: this provides favorable conditions for DM annihilation effects to play a role.

As noticed by Spolyar, Freese & Gondolo (2008), WIMP

annihilation in young haloes during the formation of the first stars could provide an amount of energy equal to the one dissipated by chemical cooling of the gas. Also, as noticed by Iocco (2008) and Freese, Spolyar & Aguirre (2008), the energy produced by DM annihilation captured inside early stars could even exceed the one produced by their nuclear burning.

Additional effects of DM decays and annihilations have also been considered in the literature, with particular attention to their contribution on the reionization and thermal histories of the intergalactic medium (Mapelli & Ferrara 2005; Ripamonti, Mapelli & Ferrara 2007a; Valdés et al. 2007) as well as on the conditions for star formation in the first mini-haloes (Ripamonti, Mapelli & Ferrara 2007b).

In this paper, we aim at studying the effects of neutralino DM annihilation on stellar evolution in the early universe. We will treat separately the effects arising from DM contraction during stellar collapse and from DM captured by scattering with the baryons: although these are clearly part of the same picture, the physical mechanisms are different and observational and experimental constraints on the parameters involved have different nature and reliability.

The paper is organized as follows: in Sec. 2 we describe the initial conditions of the model; in Sec. 3 we introduce the process of adiabatic contraction and discuss the evolution of our fiducial $100M_{\odot}$ star in the presence of this mechanism. Sec. 4 deals with the scattering/capture process and its impact on the evolution of the fiducial stellar model. In Sec. 5 we discuss the dependences on the stellar mass and DM parameters; in Sec. 6 we summarize the effects of scattering/capture process on stellar models. Finally, in Sec. 7 we discuss our conclusions. We defer to the Appendixes a synthetic description of the stellar evolutionary code and include tables with relevant physical quantities of all stellar models considered in this study.

Throughout the paper we work in the framework of a Λ cold DM (Λ CDM) cosmological model with parameters $\Omega_M = 0.24$, $\Omega_{\Lambda} = 0.76$, $\Omega_B = 0.042$, $h = 0.73$ (Spergel et al. 2007; Hinshaw et al. 2008) and we assume that DM is entirely made of neutralinos with a mass of 100 GeV.

2 INITIAL CONDITIONS

In this Section we describe our initial conditions for the density profile of the dark matter halo and for the pre-Main Sequence (pre-MS) evolution of the star. In the rest of the paper we often refer to the object under investigation as a star, or dark star, although, in most cases, it is actually a proto-star. We will make the distinction clear where necessary.

2.1 Dark matter halo

In the present study, we implement the characteristics of a “standard” early star forming mini-halo, i.e. an object with total mass $M = 10^6 M_{\odot}$ virializing at $z = 20$ (see e.g. Abel et al. 2002; Bromm et al. 2002; Yoshida et al. 2006; Gao et al. 2007; Turk 2007). We assume that 82.5% of the total mass is DM, while the rest is baryonic; DM follows a standard NFW profile (Navarro, Frenk & White 1996), with

virial radius $R_{\text{vir}} = R_{200} = 5 \times 10^{20}$ cm and concentration¹ $c = 10$. We flatten this profile for radii smaller than the free-streaming length of DM particles (6.6×10^{12} cm if their mass is 100 GeV).

It is worth noting that approximately $100M_{\odot}$ of dark matter, equivalent to the mass of the fiducial stellar model that we will discuss in the following Sections, are contained within a radius of $\approx 10^{18}$ cm. This qualitatively defines the maximum distance at which DM particles feel the gravitational pull due to the central concentration of baryons or, in other words, the maximum radius where adiabatic contraction effects are relevant, as described in Sec. 3.

2.2 Proto-star

We assume that in the first mini-haloes stars form as a result of the collapse of metal-free gas clouds, after the cooling-induced fragmentation phase is completed (see e.g. Omukai 2000 and Schneider et al. 2002). We adopt the Padova Stellar Evolution code in the version suitable for the study of zero metallicity stars (Marigo et al. 2001, 2003). A synthetic description of the code with details on the computed evolutionary tracks is presented in Appendix A1.

In order to catch the proto-star as early as possible in its evolution, within the convergence limits of the code and its physical reliability, for each stellar model we force its thermodynamic conditions to the tip of the Hayashi track by providing a density-dependent heating source; this causes an expansion of the proto-star and a drop of the effective temperature. We stress that this initial phase has no particular physical meaning; any other convenient artificial heating source would work to this purpose.

We prepare the initial conditions as follows. Starting from the configuration of a Zero Age Main Sequence (ZAMS) star of the same mass and adopting a primordial chemical composition² we then artificially expand the star towards the tip of the Hayashi track. During this artificial evolution we perform a preliminary check on the relative strengths of the DM and gravitational luminosities that, during this phase, correspond (but not exactly) to the stellar luminosity. For a $100M_{\odot}$ star, which we consider our fiducial model, the DM luminosity decreases as the baryonic configuration gets more expanded. We continue the artificial expansion until the ratio of DM annihilation to the total stellar one is $L_{\text{DM}}/L_{*} \leq 0.5$. At this stage, the central temperature is $T_c \approx 5 \times 10^4$ K and the central gas density is $\rho_c \approx 10^{-7}$ g cm⁻³. The radius of the object is $\approx 10^{14}$ cm and, according to the DM profile described in the previous Section, the enclosed DM mass is $\approx 10^{31}$ g, only 10^{-4} of the proto-stellar mass. It is difficult to push the proto-star beyond this point because of numerical problems.

Starting from this configuration, we follow the pre-MS contraction phase, including the DM annihilation energy source term in the structure equations, as described in Sections 3 and 4. It is important to stress that this model is

physically self-consistent: if gravitational energy release is the only luminosity source, the model correctly reproduces the usual track of a “standard”, non DM-burning proto-star in the HR diagram.

3 DARK MATTER CONTRACTION

As we have discussed in the previous Section, in a proto-star located at the center of the halo the DM content is $\approx 10^{-4}$ of the total mass; as a result, the DM contribution to the gravitational potential is negligible, as this is largely dominated by the baryonic mass. Starting from the initial profile described in Sec. 2.1, we evolve the density profile using the so-called adiabatic contraction (AC) approximation (Blumenthal et al. 1986), which is based on the assumption that the orbital time of the particles is much longer than the infall time (namely, orbits never cross each other). In this Section, we first introduce the formalism adopted to implement AC in our model and then describe the evolution of our fiducial $100M_{\odot}$ proto-star in the presence of DM contraction.

3.1 Formalism and approximations

The AC approximation identifies the adiabatic invariant $M(R)R$, where $M(R)$ is the mass contained within the radius R , as originally shown by Blumenthal et al. (1986). This model, which assumes spherical symmetry and circular orbits, was improved by Gnedin et al. (2004). These authors showed that, when compared to numerical simulations, the Blumenthal et al. model overpredicts the increase of DM density in the central region and that the change of the assumed invariant from $M(R)R$ to $M(\bar{R})R$ (where R and \bar{R} are the current and orbit-averaged particle positions) largely reduces the problem.

Gnedin et al. (2004) also estimate that, for $10^{-3} \lesssim (R/R_{\text{vir}}) \lesssim 1$,

$$\frac{\bar{R}}{R_{\text{vir}}} \simeq A \left(\frac{R}{R_{\text{vir}}} \right)^w, \quad (1)$$

with $A \sim 0.85 \pm 0.05$, $w \sim 0.8 \pm 0.2$. Gustaffson et al. (2006) confirmed these results, but showed that the values of A and w change from halo to halo, and that the spread is likely larger than the errors quoted above. However, in the following we used the central values ($A = 0.85$, $w = 0.8$) from Gnedin et al. (2004), as they lie well within the distribution.

With such assumptions, the modified adiabatic invariant equation is

$$R_f [M_{\text{DM},f}(\bar{R}_f) + M_{\text{b},f}(\bar{R}_f)] = R_i [M_{\text{DM},i}(\bar{R}_i) + M_{\text{b},i}(\bar{R}_i)] \quad (2)$$

where $M_{\text{DM},f}(R)$, $M_{\text{b},f}(R)$, $M_{\text{DM},i}(R)$, and $M_{\text{b},i}(R)$ are the masses of DM and baryons enclosed within a radius R , at the final (subscript f) and initial (subscript i) times. Given the initial profiles $M_{\text{DM},i}$ and $M_{\text{b},i}$ (the NFW profile described in Sec. 2.1) and $M_{\text{b},f}$ (the baryonic density given by the stellar evolution models), Eq. (2) can be solved iteratively for the radius R_f which encloses the DM mass $M_{\text{DM},i}(\bar{R}_i)$.

The numerical routine which solves the equation is

¹ We note that the “adiabatically contracted” DM profiles are almost independent of c (at least if $c \lesssim 100 - 1000$).

² We assume a H and He mass fractions of $X = 0.755$ and $Y = 0.245$, respectively, according to recent BBN models (Iocco et al. 2007).

mostly based on the public code `contra` by O. Gnedin³, although several adaptations and changes were necessary.

Finally, it is important to discuss our use of Eq. (1) down to $R \sim 10^{-7}R_{\text{vir}}$, which is well below the limit ($\sim 10^{-3}R_{\text{vir}}$) where it was tested by Gnedin et al. (2004). Although this is definitely an untested extrapolation, we think our choice is well motivated and quite conservative: the resulting central DM density is at least a factor of 10 lower than in the Blumenthal et al. (1986) model. It is worth noting that our results are in agreement with what recently found by Freese et al. (2008b): they study the density profile of an AC contracted halo, adopting two different algorithms (based on Blumenthal’s original prescription and on a modified method derived by Young (1980)); they find the two to be consistent within a factor two at baryon densities of $\mathcal{O}(10^{-11})\text{g}/\text{cm}^3$, yielding DM densities of order $10^{10}\text{GeV}/\text{cm}^3$ at radii of order 10 AU. If we use the same initial conditions and apply the algorithm based on Gnedin’s method to their baryonic profile, we find a DM density consistent within a factor three with the ones they obtain.

The specific energy deposition rate due to annihilations of DM particles is

$$\frac{dL_{\text{DM}}}{dV} = \frac{\rho^2}{m_\chi} \langle \sigma v \rangle; \quad (3)$$

where ρ is the local DM density, m_χ the neutralino mass, $\langle \sigma v \rangle$ the thermally-averaged annihilation rate. We adopt $\langle \sigma v \rangle = 3 \times 10^{-26} \text{cm}^3 \text{s}^{-1}$ which best fits the current value of the DM relic density (Bertone et al. 2005). DM particles in the halo are strongly non-relativistic: therefore the p-wave term, which contributes to the annihilation rate in the early Universe, is negligible in astrophysical environments; this may lead to different values of $\langle \sigma v \rangle$. In general, however, the same value we adopt is taken as “fiducial” in DM indirect search studies (see e.g. Fornengo, Pieri & Scopel 2004). We also assume the neutralino mass to be $m_\chi = 100 \text{GeV}$; we will discuss the effects of the variation of these parameters in Sec. 5. In general, only a fraction f of the energy released in the annihilation is emitted in form of particles that can be thermalized by the gas; we take $f = 2/3$, as for a typical neutralino annihilation $\approx 1/3$ of the energy goes into neutrinos (Bertone et al. 2005), and the rest of hadronic and electromagnetic shower induced by the primaries fastly thermalizes inside the protostellar core, as estimated by Spolyar et al. (2008) for even lower baryonic densities⁴.

3.2 Proto-star evolution with DM contraction

We now turn to a detailed discussion of the DM effects on the evolution of a $100 M_\odot$ proto-star, which we take to be our fiducial model deferring to Sec. 5 the study of different masses. We anticipate that, qualitatively, the conclusions and the physical picture we draw in this Section do not depend strongly on the assumed stellar mass.

The initial NFW profile described in Sec. 2.1 is adiabatically contracted, as described in the previous Section, in

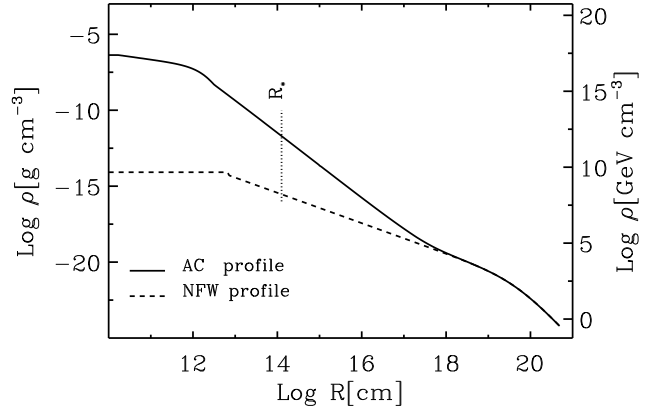


Figure 1. Initial NFW DM density profile of adopted $M = 10^6 M_\odot$ halo (dashed line) and adiabatically contracted DM profile at the time of our initial proto-stellar phase of for the fiducial $100 M_\odot$ star. The vertical dashed line marks the radius of the star at the beginning of the computation.

order to obtain a configuration in which the baryonic component would correspond to our initial proto-stellar phase, at the tip of the Hayashi track, presented in Sec. 2.2. The initial NFW profile of the halo, and the AC contracted DM density distribution at the time we start our simulation are shown in Fig. 1; the dramatic enhancement (approximately seven orders of magnitude within the central 10^{12}cm) of DM density is the cause of the pronounced effects of DM annihilation that will be discussed in the following.

The corresponding DM profile at this point is let evolve together with our stellar object, whose evolution follows a typical track in the HR diagram: the proto-star is totally convective and contracts on a Kelvin-Helmholtz time scale (approximately 10^2yr in this phase), descending the Hayashi track. For reference, the track of a $100 M_\odot$ (together with other stellar masses) in the HR diagram is reported in Fig 5.

The DM annihilation luminosity (AC luminosity) becomes the dominant component of the total luminosity on a very short timescale ($\approx 10 \text{yr}$). Although the mass of DM contained inside the star at this point is only $\approx 10^{31}\text{g}$, 10^{-4} of its baryonic mass (and 10^{-8} of the total mass of the halo), the luminosity arising from the annihilations of the DM concentrated within the central $\approx 2 \times 10^{11}\text{cm}$ is large enough to sustain the star, causing a *stalling phase*. This kind of object has been named a *dark star* by Spolyar et al. (2008), who first found that DM annihilation energy release can counteract the gravitational collapse at some point during the pre-stellar phase.

Once the proto-stellar contraction has stalled, due to the energy released by DM annihilations, the contraction of the DM profile is inhibited as well. Part of the DM in the cusp is burned by annihilations causing a luminosity drop, followed by a small contraction of the baryons and DM which re-establishes a new equilibrium state. In reality, this sequence of stable equilibrium states along the Hayashi track represents a continuous process which is eventually terminated when the DM density in the cusp has decreased below the threshold at which the energy input can no longer sustain the self-gravity pull, i.e when the annihilation timescale

³ See <http://www.astro.lsa.umich.edu/~ognedin/contra/>

⁴ It is worth noting that the mean free path for electrons and photons with energy lower than the neutralino mass m_χ , is much smaller than the radius of the star at any time during our analysis.

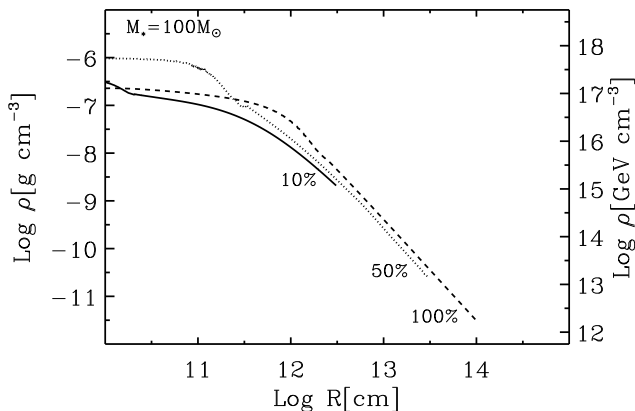


Figure 2. DM density profile, truncated at the stellar radius, R_* , at different stages during the pre-MS evolution of the fiducial $100M_\odot$ proto-star. Curves are labelled by the ratio L_{DM}/L_* ; conversion to corresponding time and temperatures can be read off Fig. 3.

becomes longer than the local Kelvin-Helmholtz time. The duration of the stalling phase, τ_{AC} , is defined as the time needed to the AC luminosity to scale down to 50% of the stellar luminosity, i.e. $L_{\text{DM}}/L_* = 0.5$, and it is much longer than the typical Kelvin-Helmholtz timescale. For our fiducial set of parameters (recall this is degenerate in the ratio $\langle\sigma v\rangle/m_\chi$), the $100M_\odot$ dark star stalls for $\tau_{\text{AC}} = 5.3 \times 10^3$ yr.

In Fig. 2 we show the DM density profile inside R_* at different stages of the proto-stellar evolution, benchmarked by the fraction of stellar luminosity provided by AC luminosity, L_{DM}/L_* . The contraction and subsequent flattening of the central cusp with respect to the initial conditions of the stalling phase, where $L_{\text{DM}}/L_* = 1$, together with the progressive shrinking and the loss of DM annihilating shells, is the reason of the efficiency decrease of the AC luminosity. The central enhancement of the central cusp at the 50% stage with respect to the 100%, dark star phase, is not able to compensate the loss of the external shells of annihilating DM.

Fig. 3 shows the time evolution of the effective temperature for different proto-stellar masses. During the stalling phase, the dark star is kept stable on the HR diagram by the DM energy production (which is temperature independent) and it remains cool $T_{\text{eff}} \approx 5 \times 10^3$ K, as can be seen from the initial plateau visible in the bottom left corner of the Figure. When the DM cusp is exhausted, the dark star evolves along its pre-MS track with characteristic times longer than for a standard, non DM-supported, stellar model of the same mass, due to the additional support of AC luminosity. Fig. 3 restates the results that the dark star exits the stalling phase in $\tau_{\text{AC}} = 5.3 \times 10^3$ yr, and reaches the bottom of the Hayashi track in $\tau_{\text{Hay}} = 4.4 \times 10^3$ yr. By comparison a standard, non DM-supported, star of the same mass reaches the same point in $\tau_{\text{Hay}}^0 \approx 60$ yr. Table 1 shows these characteristic timescales for a grid of stellar mass models.

This might have interesting implications for the radiative feedback effects of the dark star on its host and nearby haloes, as we will discuss in our Conclusions.

4 DARK MATTER CAPTURE

If DM is made of weakly interacting massive particles, a non-vanishing elastic scattering cross section between DM and baryons arises. WIMPs scattering off the nuclei which constitute the star lose part of their energy and some of them remain bound by gravitational attraction. In this Section, we first introduce the formalism necessary to implement scattering/capture (SC) process in the code and then we discuss their effects on the evolution of our $100M_\odot$ fiducial proto-stellar model.

4.1 Formalism and approximations

The capture rate, C , of DM particles by a star through scattering has been calculated by Gould (1987), and can be cast as follows:

$$C = 4\pi \int_0^{R_*} dR R^2 \frac{dC(R)}{dV}, \quad (4)$$

where

$$\begin{aligned} \frac{dC(R)}{dV} &= \left(\frac{6}{\pi}\right)^{1/2} \sigma_0 A_n^4 \frac{\rho_*}{M_n} \frac{\rho}{m_\chi} \frac{v^2(R)}{\bar{v}^2} \frac{\bar{v}}{2\eta A^2} \\ &\times \left\{ \left(A_+ A_- - \frac{1}{2} \right) [\chi(-\eta, \eta) - \chi(A_-, A_+)] \right. \\ &\left. + \frac{1}{2} A_+ e^{-A_-^2} - \frac{1}{2} A_- e^{-A_+^2} - \eta e^{-\eta^2} \right\}, \\ A^2 &= \frac{3v^2(R)\mu}{2\bar{v}^2\mu_-^2}, \quad A_\pm = A \pm \eta, \quad \eta = \sqrt{\frac{3v^2}{2\bar{v}^2}}, \\ \chi(a, b) &= \int_a^b dy e^{-y^2} = \frac{\sqrt{\pi}}{2} [\text{erf}(b) - \text{erf}(a)], \end{aligned} \quad (5)$$

σ_0 is the DM-baryon elastic scattering cross section, A_n (M_n) is the atomic number (mass) of stellar nuclei, ρ is the ambient WIMP density, \bar{v} is the WIMP velocity dispersion, v_* is the velocity of the star with respect to the observer, $v(R)$ is the escape velocity at a given radius R inside the star, $\mu = m_\chi/M_n$, $\mu_- = (\mu - 1)/2$, and the subscript $*$ refers to stellar quantities. The factor η is usually assumed to be $\sqrt{3/2}$, corresponding to the condition $v_* = \bar{v}$. WIMPs captured by the scattering process thermalize with the gas; an upper limit to the thermalization time can be estimated as $(m_\chi/m_p)(\lambda_\chi/v_\chi)$, i.e. the WIMP-proton mass ratio (number of scatterings needed) times the WIMP mean free path divided by its dispersion velocity in the star (we take v_χ equal to the escape velocity at the stellar surface), thus obtaining:

$$\tau_{\text{th}} = \frac{4\pi}{3\sqrt{2G}} \frac{m_\chi}{\sigma_0} \frac{R_*^{7/2}}{M_*^{3/2}}. \quad (6)$$

Assuming that the energy of the DM particles is in equilibrium with the gravitational field of the star, their number density follows a Maxwell-Boltzmann distribution (Griest & Seckel 1987),

$$n_\chi(R) = n_\chi^c \exp(-R^2/R_\chi^2), \quad n_\chi^c = \frac{C\tau_\chi}{\pi^{3/2}R_\chi^3}; \quad (7)$$

where n_χ^c is the highest DM density achievable inside the star once equilibrium between capture and annihilation is reached after a time

$$\tau_\chi = \left(\frac{\pi^{3/2} R_\chi^3}{C \langle \sigma v \rangle} \right)^{1/2}. \quad (8)$$

The radius within which captured DM is concentrated, once it has thermalized with the star, reads

$$R_\chi = c \left(\frac{3kT_c}{2\pi G \rho_c m_\chi} \right)^{1/2}, \quad (9)$$

where T_c and ρ_c are the stellar core temperature and density, respectively.

The energy released due to annihilations *inside* the star can be self-consistently computed once the profile $n_\chi(R)$ is known. The expression for such quantity given in Eq. (7) assumes that particles are thermalized and equilibrium between annihilation and capture processes has been reached. To take into account the transient phase before WIMPs settle to such a state, we write the annihilation luminosity as,

$$L_{\text{DM}}(t) = g(t) 4\pi f \int_0^{R_*} dR R^2 n_\chi^2(R) \langle \sigma v \rangle m_\chi, \quad (10)$$

with $g(t) = \tanh^2(t/\tau_{\text{dyn}})$, where $\tau_{\text{dyn}} = \max(\tau_\chi, \tau_{\text{th}})$; this is a formal solution when $\tau_\chi > \tau_{\text{th}}$, and otherwise still represents a good approximation to deal with a transient, reducing to the exact solution, $L_{\text{DM}} = C m_\chi f$, when $t > \tau_{\text{th}}$. Finally, f is the fraction of released energy absorbed within the star, which we take to be 2/3 for a typical neutralino annihilation, as discussed in Sec. 3.

The process we have described presents some peculiarities which are worth discussing. Although the physical energy source is the annihilation process, its rate is controlled by scattering processes which governs the capture rate. Its dependence on the background WIMP density is only linear (rather than quadratic, as in the case of annihilation reactions), and it depends on σ_0 rather than on $\langle \sigma v \rangle$. As it can be appreciated from Eqs. (7) and (8), $\langle \sigma v \rangle$ and m_χ affect the τ_χ and n_χ^c , but within the region of the parameter space which is relevant to this problem they do not affect the final DM luminosity.

Eq. (5) should be integrated for each single atomic species in the star. However, if one relies on the current experimental upper limits for DM direct detection for a 100 GeV mass neutralino, namely $\sigma_0^d = 10^{-38} \text{cm}^2$ (Desai et al. 2004⁵ and Angle et al. 2008⁶), and $\sigma_0^i = 4 \times 10^{-44} \text{cm}^2$ (Ahmed et al. 2008⁷), the capture rate is negligible for any species but hydrogen. In stars of primordial composition, such as Pop III ones, even the dependence on the coherence factor A_n^4 does not introduce any significant contribution of elements other than hydrogen. Our choice for the cross section values is in agreement with other works in the literature, i. e. (Moskalenko & Wai 2007; Bertone & Fairbairn 2008; Fairbairn et al. 2008).

Throughout the following we adopt $\bar{v} = 10 \text{ km s}^{-1}$, which represents the virial velocity of our reference mini-halo with mass $10^6 M_\odot$ at redshift $z \approx 20$.

By integrating Eq. (5) with a flat stellar density profile, one obtains a simplified expression for the capture rate,

$$C \propto \sigma_0 M_* v_{\text{esc}}^2 \frac{\rho}{m_\chi} = C_0 \sigma_0 \frac{M_*^2}{R_*} \frac{\rho}{m_\chi}. \quad (11)$$

which, within the precision of experimental data, corresponds to a numerical estimate of,

$$C = 9.2 \times 10^{47} \text{s}^{-1} \frac{M_*^2}{R_*} \frac{\rho_{11} \sigma_{38}}{m_{100}}, \quad (12)$$

having defined:

$$\rho_{11} = \frac{\rho}{10^{11} \frac{\text{GeV}}{\text{cm}^3}}; \quad \sigma_{38} = \frac{\sigma_0}{10^{-38} \text{cm}^2}; \quad m_{100} = \frac{m_\chi}{100 \text{GeV}}, \quad (13)$$

and expressing M_* in solar masses and R_* in cm.

It follows that, at equilibrium,

$$L_{\text{DM}} = 1.4 \times 10^{47} \frac{\text{erg}}{\text{s}} \frac{M_*^2}{R_*} \frac{\rho_{11} \sigma_{38}}{m_{100}}. \quad (14)$$

In the above expression we have taken $f = 2/3$ (see discussed in Sec. 3). Eq. (14) predicts that for a given mass M_* , L_{DM} will grow during stellar contraction, potentially reaching a level able to halt the collapse. In the code, we have implemented a term of DM luminosity due to annihilations of captured WIMPs (SC luminosity) using Eq. (14) multiplied by the transient factor $g(t)$ described in Eq. (10).

We emphasize that the process of DM capture is sensitive to the background DM density outside the star but not to the DM already accreted through adiabatic contraction. Thus, the two processes are mutually independent. Moreover, scattering/capture processes can continue for long times: in a $10^6 M_\odot$ halo, a DM luminosity of $10^{41} \text{ erg s}^{-1}$ can be sustained for approximately 10^{12} yr .

4.2 Proto-star evolution with DM capture

We follow the evolution of our reference $100 M_\odot$ proto-star, after the stalling phase due to the AC luminosity described in Sec. 3.2. The fiducial DM parameters are $\sigma_0 = 10^{-38} \text{cm}^2$ and $\rho = 10^{11} \text{GeV/cm}^3$, which is the value set by adiabatic contraction in the vicinity of the star ($R \lesssim 10^{15} \text{cm}$), as shown in Fig. 1. It is worth noticing that this value of ρ closely matches the one predicted by 3D simulations of first star formation (Turk 2007). We will discuss the dependence of our model results on these parameter in Sec. 5.

At the time of stallation, the radius of the dark star is $R_* \approx 10^{14} \text{cm}$. Once the DM density cusp generated through AC is exhausted, the energy released by DM annihilations is no longer sufficient to stop the gravitational collapse; also, the SC luminosity developed at this point is, at the equilibrium⁸, approximately 10^{37} erg/s , as it can be calculated with Eq. (14). The dark star continues its evolution along the Hayashi line and in the pre-MS phase.

While the star shrinks and evolves leftward on its track in the HR diagram, the capture rate grows as can be seen in Fig. 4, where we show the contributions to the total stellar luminosity of the different processes as a function of the stellar age. As shown in the Figure, despite the fact that SC DM annihilations are dominating the overall luminosity, at times $> 2 \times 10^3 \text{ yr}$, nuclear reactions are active producing a luminosity of $L_{\text{nuc}} \approx 2 \times 10^{38} \text{ erg/s}$ ($10^5 L_\odot$), eventually

⁵ SuperKamiokande Collaboration

⁶ XENON10 Collaboration

⁷ CDMS Collaboration

⁸ We note that $\tau_{\text{th}} \approx 10^{10} \text{yr}$ at this stage, thus making the actual SC luminosity even smaller than its equilibrium value.

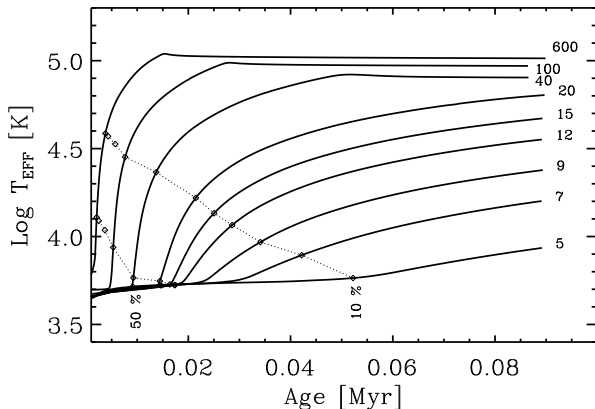


Figure 3. Evolution of the effective temperature for a selected set of stellar models when only the effects of AC DM annihilations is considered. The dotted lines indicate the evolutionary stages of the stars when the AC DM luminosity has decreased to 50% and 10% of the total stellar luminosity.

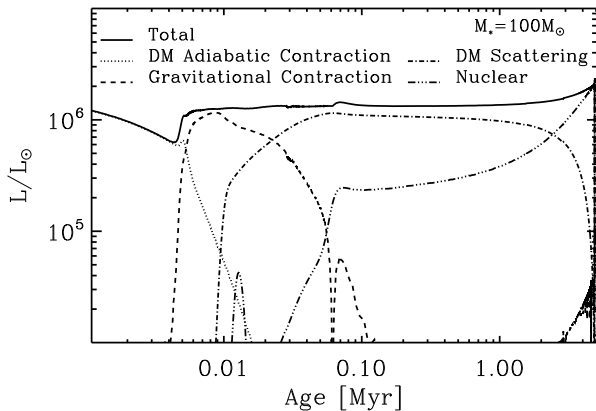


Figure 4. Total luminosity of our reference $100M_{\odot}$ star as a function of its age. The different curves show the contribution from AC DM annihilations (dotted line), gravitational contraction (short dashed), SC DM annihilations (dot-dashed), nuclear reactions (dot-dot-dot-dashed). Where relevant, the processes have been computed for our fiducial values of σ_0 and ρ (see text).

leading the star to exhaust the hydrogen into its core and continue its evolution, although with longer timescales. We have followed the evolution of our fiducial stellar model until complete consumption of helium in the stellar core. The hydrogen burning lifetime is $\tau_{\text{H}} = 4.9$ Myr, to be compared with the $\tau_{\text{H}}^0 = 2.6$ Myr predicted for a Pop III star of the same mass in the absence of DM effects (see Table 2). The helium burning lifetime remains essentially unchanged.

Thus, the evolution of the star is slower than what expected for a star of the same mass in the absence of DM capture.

As we will show in the next Section, lower mass stars are more sensitive to DM effects and for this same set of parameters they actually stop before getting to the ZAMS.

5 PARAMETER VARIATION

In this Section we will discuss the dependence of model results on the assumed parameters. In particular, we will explore (i) a grid of stellar masses and (ii) different DM parameters. We will consider these in turn.

We find that all stars stall very early in their evolution, when they all stand on the Hayashi track (namely, they are entirely convective). The evolution of the effective temperature during the AC phase for a few selected stellar models is shown in Fig. 3, where the dotted lines mark the evolutionary stages where the AC luminosity has decreased to 50% and 10% of the total stellar luminosity. As can be inferred from the Figure, larger masses burn their DM content more rapidly than smaller ones. In Table 1, we report the characteristic timescale of the AC phase and the time taken by each star to reach the bottom of the Hayashi track with (τ_{Hay}^0) and without ($\tau_{\text{Hay}}^{\text{DM}}$) the contribution of AC luminosity for the whole range of stellar masses under investigation. The duration of the stalling phase induced by the AC luminosity varies with stellar mass M_* , ranging from 2.1×10^3 yr for a $600M_{\odot}$ star to 1.8×10^4 yr for a $9M_{\odot}$ star.

We have not been able to explore a wide range of values for $\langle\sigma v\rangle/m_{\chi}$ for problems of numerical convergence; however, we have performed a run for our fiducial value of the annihilation rate and a neutralino mass $m_{\chi} = 200$ GeV. Results are reported in the Appendix A2, and show that for higher values of the neutralino mass (or smaller values of the annihilation rate) the delaying effect of the AC luminosity is reduced: the smaller amount of energy per unit time makes the contraction of the star faster.

Fig. 5 shows the evolution of different stellar models in the HR diagram. The results presented in the upper panel have been obtained using our fiducial DM parameters, namely $\sigma_0 = 10^{-38} \text{cm}^2$ and $\rho = 10^{11} \text{GeV cm}^{-3}$. The dotted lines mark the position of the star when $L_{\text{DM}}/L_* = 1$ (i.e. at the beginning of the stalling phase), 0.5 and 0.1. As already discussed, for all the considered stellar models the stalling phase takes place along the Hayashi track, and the timing of the other benchmarked points can be inferred by comparison with Fig. 3.

Following the stalling phase, these dark stars continue their contraction. The SC mechanism becomes more relevant as the density increases, and the SC rate grows. For our fiducial set of DM parameters, stars with $M_* \lesssim 30M_{\odot}$ develop a SC luminosity greater than the gravitational one before reaching the ZAMS, and therefore do not evolve further on the HR diagram. This is clearly shown in the upper panel of Fig. 5, where the dashed tracks, which indicate the pre-MS phase, do not join the main sequence (solid lines) for all stellar models with $M_* \leq 20M_{\odot}$. The lower panel of the Figure shows the HR diagram of the same set of stellar models but assuming different DM parameters, namely $\sigma_0 = 10^{-39} \text{cm}^2$ and $\rho = 10^{11} \text{GeV cm}^{-3}$. As expected, the evolution is almost unaffected by the variation of DM parameters during the AC phase whereas the SC effects are significantly reduced: all the stars with $M_* > 5M_{\odot}$, reach the main sequence and even the evolution of the $5M_{\odot}$ model is halted at a later time with respect to the previous case.

In Table 2, we summarize the characteristic timescales which characterize the evolution of our stellar models under the effect of SC assuming different DM cross sections,

Table 1. Characteristic times of the star relative to the phase induced by the AC luminosity. The adiabatic time τ_{AC} has been defined as the time needed to the AC DM annihilation luminosity, L_{DM} to scale down to 50% of the total stellar luminosity L_* . We also report the stellar radii R_{AC} . The last two columns show the time required to reach the bottom of the Hayashi track from its tip with (τ_{Hay}) and without (τ_{Hay}^0) AC DM annihilation.

$M(M_{\odot})$	$\tau_{\text{AC}}(10^3\text{yr})$	$R_{\text{AC}}(\text{cm})$	$\tau_{\text{Hay}}(\text{yr})$	$\tau_{\text{Hay}}^0(\text{yr})$
5	9.7	4.0×10^{13}	3.2×10^4	1.8×10^4
7	15	4.6×10^{13}	2.1×10^4	6.9×10^3
9	18	5.0×10^{13}	1.8×10^4	3.5×10^3
12	18	5.6×10^{13}	1.5×10^4	1.6×10^3
15	16	6.1×10^{13}	1.4×10^4	1.0×10^3
20	14	6.8×10^{13}	1.2×10^4	5.6×10^2
40	9.3	9.0×10^{13}	8.2×10^3	2.0×10^2
100	5.3	1.2×10^{14}	4.4×10^3	62
200	3.7	1.6×10^{14}	2.5×10^2	26
400	2.5	2.1×10^{14}	95	13
600	2.1	2.4×10^{14}	45	3.9

as compared with the standard case where DM effects are neglected: once again it is evident the bigger impact of the SC mechanism on smaller masses and the life-prolonging effect of DM on all the masses.

6 STELLAR MASS CONSTRAINTS

From the above picture, it is clear that in DM-rich environments, such as the haloes where the first episodes of star formation are expected to take place, SC luminosity may play a dramatic role during the early evolution of a proto-star. On the basis of purely quantitative arguments, this has been suggested by Iocco (2008), and Freese et al. (2008) derived a constraint on the mass of stars that can form under these conditions. Our analysis reaches conclusions that are different from those of the latter study as we will comment later in this Section. Now we want to answer the question of which stars will be most affected by this mechanism, and in which environment. Armed with the formalism developed in Sec. 4, one may simply impose the condition $L_{\text{DM}}^{\text{ZAMS}} \leq L_{\text{nucl}}^{\text{ZAMS}}$, namely that the luminosity due to DM annihilations inside the star be less than the nuclear luminosity predicted at ZAMS for Pop III stars in the absence of dark matter. Fig. 6 summarizes the results of this disequation, obtained by applying Eq. (14) to a grid of stellar models at the ZAMS.

In the region above the curve, DM luminosity exceeds the nuclear one and proto-stellar evolution is inhibited before the objects reach the ZAMS, as we have discussed in the previous Section. Stars in this regime will “freeze” on the HR diagram as long as the properties of the DM distribution around them remain the same. Below the curve (shaded area) stars are instead able to reach the ZAMS and thereafter evolve along the main sequence.

Note, however, that the distinction between “frozen” and “evolving” stars has to be taken with care. In fact, as we have shown in Fig. 4 for our reference $100 M_{\odot}$ stellar model, the ignition of nuclear reactions can occur at very low rates, producing a very low nuclear luminosity, but still allowing the star to evolve, eventually exhausting its nuclear fuel, although on much longer timescales ($\tau_{\text{H}} = 4.9$ Myr against the $\tau_{\text{H}}^0 = 2.6$ Myr timescale predicted for a $100 M_{\odot}$ Pop III star in the absence of DM effects, see Table 2).

Fig. 6 has to be considered as a quantitative indication: it shows that both low and high mass stars are affected by DM capture. The range of stellar masses that can reach the ZAMS, for the fiducial DM parameter combination ($\sigma_0 \rho = 10^{-27}$ GeV/cm), is $40 M_{\odot} \lesssim M_* \lesssim 1000 M_{\odot}$.

This is due to a change in the index k of the relation $L_* \propto M_*^k$, following the transition of the star to a completely adiabatic system when $M_* \gtrsim 200 M_{\odot}$. In their analysis, Freese et al. (2008) derive only an upper limit to the stellar mass in the presence of DM SC because they impose the above condition making use of the Eddington luminosity, which has a linear dependence on the stellar mass, instead of the actual nuclear luminosity at ZAMS. Therefore their analysis somehow under-predicts the effects of DM on low and intermediate mass stars. In fact, our numerical results show that most significant effects are obtained for objects with masses $M_* \lesssim 200 M_{\odot}$, as shown in Fig. 6. This happens because the SC mechanism becomes efficient only when the stars are in a relatively advanced phase of their pre-MS evolution.

It is also extremely interesting to notice that the mass-luminosity relation in low-mass stars is not particularly sensitive to metallicity. This implies that the results we have presented can be also applied to metal-enriched stellar populations, as long as they continue to form in environments with characteristics similar to those we have considered (see Sec. 2). Our results are in agreement with those of Salati & Silk (1989), Fairbairn et al. (2008) and Scott et al. (2007), who studied the main sequence evolution of WIMP-burning stars and observed that ZAMS stars, if “fed” with captured DM annihilation energy move towards the red region of the HR diagram, at increasing DM densities. In particular, the latter analysis focused on low-mass stars ($M_* \leq 4 M_{\odot}$) and found they eventually reach the Hayashi line for different DM density values at different masses ($\rho = 10^{10}$ GeV/cm³ for $1 M_{\odot}$), using the same current upper limit on σ_0 we adopt, and a different value for \bar{v} , of the order of the relative velocity between WIMPs and Sun, $\bar{v} \sim \mathcal{O}(10^2 \text{ Km/s})$.

Table 2. Times needed to nuclear luminosity L_{nuc} to be 95% of the total L_* , τ_Z ; τ_H is the time at which the hydrogen is totally exhausted in the core; underscored 0 refers to the case of complete absence of any dark matter annihilation mechanism. $\sigma_{38}(\sigma_{39})=10^{-38}(10^{-39})$ cm^2 , $\rho=10^{11}\text{GeV}/\text{cm}^3$.

$M(M_\odot)$	$\tau_Z^0(10^3\text{yr})$	$\tau_Z(10^3\text{yr})(\sigma_{39})$	$\tau_Z(10^3\text{yr})(\sigma_{38})$	$\tau_H^0(\text{Myr})$	$\tau_H(\text{Myr})(\sigma_{39})$	$\tau_H(\text{Myr})(\sigma_{38})$
7	4.9×10^2	5.8×10^4	Stalling	29	60	Stalling
9	4.0×10^2	3.1×10^4	Stalling	20	33	Stalling
12	2.0×10^2	1.6×10^4	Stalling	14	18	Stalling
15	1.5×10^2	1.1×10^4	Stalling	11	13	Stalling
20	1.0×10^2	6.4×10^3	Stalling	7.7	8.6	Stalling
40	41	2.4×10^3	2.1×10^4	4.1	4.4	21
100	22	1.1×10^3	4.6×10^3	2.6	3.0	4.9
200	17	9.6×10^2	3.6×10^3	2.2	2.4	3.9
400	14	1.1×10^3	3.4×10^3	2.0	2.0	3.7
600	13	9.7×10^2	4.0×10^3	2.1	2.0	4.1

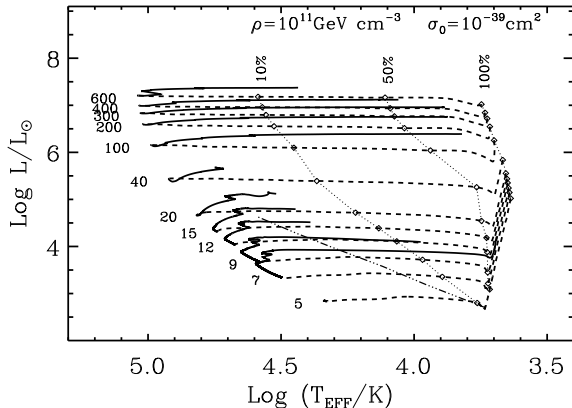
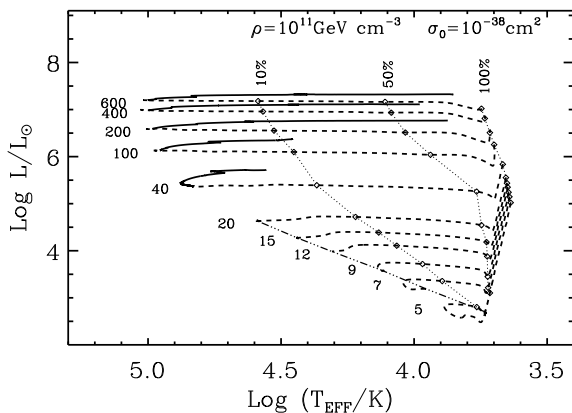


Figure 5. The HR diagram for a grid of stellar masses. For each stellar model, the dashed line represents the pre-MS phase and the solid line represent the MS. Dotted diagonal lines mark the evolutionary stages when $L_{\text{AC}}/L_* = 1, 0.5$ and 0.1 . The dot-dashed line illustrate the locus of the “freezing” points, when the evolution is halted by SC DM annihilation luminosity before the ZAMS. In the *upper* panel, the results have been obtained using our fiducial DM parameters, namely $\sigma_0 = 10^{-38}\text{cm}^2$ and $\rho = 10^{11}\text{GeV cm}^{-3}$. The small loops in the 5 and $7 M_\odot$ models are due to the effect of WIMPs thermalization, which results in an effective delay of the effects of SC DM annihilation luminosity. In the *lower* panel, the stellar models have been run assuming the same DM density but $\sigma_0 = 10^{-39}\text{cm}^2$.

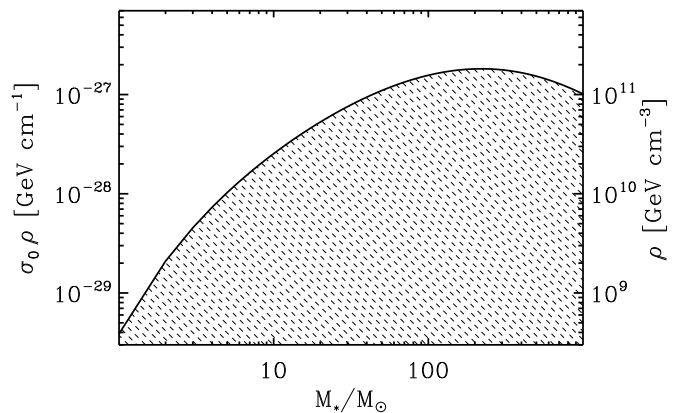


Figure 6. Dark matter constraints on stellar mass. The shaded area represents the region of the parameter space where stars can reach the ZAMS and evolve. The vertical axis on the left represents the quantity $\sigma_0 \rho$ and on the right the corresponding values of ρ if $\sigma_0 = 10^{-38}\text{cm}^2$. In the region above the curve, stars are prevented from reaching ZAMS and freeze on the HR diagram, as it is shown in Fig. 5.

7 CONCLUSIONS

We have studied the effects of WIMP dark matter annihilation on the first stars in the Universe. As initial condition of our model, we consider a dark matter halo with mass $10^6 M_\odot$ at $z = 20$, i.e. a typical mini-halo where the first star formation episodes are expected to occur. We have treated separately the mechanism of adiabatic contraction (AC) and scattering/capture (SC) and highlighted their effects on the pre-Main Sequence (pre-MS) phase of stellar objects with masses $5 M_\odot < M_* < 600 M_\odot$ formed from the collapse of metal-free gas clouds. We find that:

- Early in the proto-stellar evolution, the luminosity produced by DM annihilations during the AC regime induces a transient stalling phase: all the proto-stars become *dark* stars for characteristic times ranging from $2.1 \times 10^3\text{yr}$ for a $600 M_\odot$ star to $1.8 \times 10^4\text{yr}$ for a $9 M_\odot$ star.
- The stalling phase occurs when the stars are on the Hayashi track. The AC luminosity does moderate the effective temperature of the star, by enabling an equilibrium state at the early evolutionary stages, characterized

by larger radii, when the effective temperature is $\approx 5 \times 10^3$ K.

Later in the evolution, the capture of WIMPs by means of scattering on the baryonic matter of the star becomes high enough that WIMPs accumulated and annihilating inside it produce enough energy to keep the object at equilibrium. The details of this depend on environmental conditions of DM, elastic scattering cross section between WIMPs and baryons, and mass of the star.

For our fiducial set of parameters ($\bar{v}=10$ km/s, $\rho=10^{11}$ GeV/cm³, $\sigma_0=10^{-38}$ cm²), we find that:

- Small and intermediate mass stars ($M_* < 40M_\odot$) are most affected by SC luminosity and their evolution is halted on the HR diagram before reaching the ZAMS.
- *Dark* stars can be supported by SC luminosity as long as the environmental conditions remain unaltered. This is because, unlike the AC mechanism, SC luminosity depends on the flux of DM particles streaming through the star from outside, thus drawing from a virtually unexhaustable reservoir: *dark* stars remain “frozen” on the HR diagram.
- Stars with masses $\geq 40M_\odot$ manage to ignite nuclear reactions, and go through the Main Sequence supported by an additional energy source: dark matter “burning” prolongs their lifetimes from a factor 2 for a $600M_\odot$ to a factor 5 for a $40M_\odot$ star.

These conclusions depend on the assumed dark matter parameters and on the specific environment where the first stars are expected to form. However, they do not strongly depend on the assumed primordial chemical composition of the stars. Thus, they can be applied to more evolved stellar populations as long as the characteristics of the environment where these stars form are similar to the ones we have considered.

The existence of *dark* stars can have many interesting consequences for a number of issues. In fact, once they are frozen on the HR diagram, they have effective temperatures in the range $10^4 - 10^5$ K and provide a continuous source of UV photons. This could have interesting consequences for the radiative feedback on the parent and neighbouring haloes as well as on the reionization history. The duration of this *dark* stellar phase is difficult to estimate, as it depends on the persistence of high dark matter densities around the stars. Therefore, their fate is strictly related to the evolution of their parent dark matter haloes and their merger histories.

Of course, the present analysis represents only a first step of more refined future studies; however, it opens a relatively novel window on high redshift star formation. Progresses on the issues discussed here might lead to considerable understanding of the signatures that the yet mysterious dark matter particles have unmistakably left on the stars that formed in the baby Universe.

ACKNOWLEDGEMENTS

F. I. acknowledges support from the grant COFIN-MIUR Pacini2006. A. B. and P. M. acknowledge financial contribution from contract ASI I/016/07/0.

We thank G. Bertelli, L. Girardi, and M. Mapelli for stimulating discussions. F. I. thanks M. Fairbairn and P. Scott for useful conversations.

REFERENCES

- Abel T., Anninos P., Norman M., Zhang Y., 2000, ApJ, 508, 518
 Abel T., Bryan G. L., Norman M. L., 2002, Science, 295, 93
 Ahmed Z. *et al.* [CDMS Collaboration], arXiv:0802.3530 [astro-ph]
 Alexander D. R., Ferguson J. W., 1994, ApJ, 437, 879
 Alongi M., Bertelli G., Bressan A., Chiosi C., 1991, A&A, 244, 95
 Amin M. A., Wizansky T., arXiv:0710.5517 [astro-ph]
 J. Angle *et al.*, arXiv:0805.2939 [astro-ph]
 Barkana R., Loeb A., 2001, Phys. Rep. 349, 125
 Bertone G., Hooper D., Silk J., 2005, Phys. Rep. 405, 279
 Bertone G., Fairbairn M., 2008, Phys. Rev. D, 77, 043515
 Blumenthal G. R., Faber S. M., Flores R., Primack J. R., ApJ, 1986, 301, 27
 Böhm-Vitense E., Z. Astroph. , 1958, 46, 108
 Bressan A., Bertelli G., Chiosi C., 1981, A&A, 102, 25
 Bromm V., Coppi P. S., Larson R. B., 1999, ApJ, 527, L5
 Bromm V., Ferrara A., Coppi P. S., Larson R. B., 2001, MNRAS, 328, 969
 Caughlan G. R., Fowler W. A., 1988 At. Data Nucl. Data Tables, 40, 283
 Choudhury T. R., Ferrara A., 2006, MNRAS, 371, L55
 Ciardi B., Ferrara A., 2005, Space Science Rev., 116, 625
 Desai S. *et al.* [Super-Kamiokande Collaboration], 2004, Phys. Rev. D, 70, 109901
 Eke V. R., Navarro J. F., Steinmetz M., 2001, ApJ, 554, 114
 Fairbairn M., Scott P., Edsjo J., 2008, Phys. Rev. D, 77, 047301
 Fornengo N., Pieri L., Scopel S., 2004, Phys. Rep. D, 70, 103529
 Freese K., Spolyar D., Aguirre A., arXiv:0802.1724 [astro-ph]
 Freese K., Gondolo P., Sellwood J. A., Spolyar D., [Freese et al. (2008b)] arXiv:0805.3540 [astro-ph]
 Gao L., Abel T., Frenk C. S., Jenkins A., Springel V., Yoshida N., 2007, MNRAS, 378, 449
 Girardi L., Bressan A., Bertelli G., Chiosi C., 2000, A.&A, 141, 1
 Gnedin O. Y., Kravtsov A. V., Klypin A. A., Nagai D., 2004, ApJ, 616, 16
 Gnedin N., Fan X., 2006, ApJ, 648, 1
 Gould A., 1987, ApJ, 321, 571
 Graboske H.C., de Witt H.E., Grossman A.S., Cooper M.S., 1973, ApJ, 181, 457
 Griest K., Seckel D., 1987, Nucl. Phys. B 296, 681
 Gustafsson M., Fairbairn M., Sommer-Larsen J., 2006, Phys. Rev. D, 74, 123522
 Haft M., Raffelt G., Weiss A., 1995, ApJ, 425, 222
 Heger A., Woosley S. E., 2002, ApJ, 567, 532
 Hubbard W. B., Lampe M., 1969, 18, 297
 Iglesias C.A., Rogers F.J., 1993, ApJ, 412, 752
 Iocco F., Mangano G., Miele G., Raffelt G. G., Serpico P. D., 2005, Astropart. Phys. , 23, 303
 Iocco F., Mangano G., Miele G., Pisanti O., Serpico P.D., 2007, Phys. Rev. D, 75, 087304
 Iocco F., Murase K., Nagataki S., Serpico P.D., 2008, ApJ, 675, 937
 Iocco F., 2008, ApJ, 677, L1
 Itoh, N., Mitake, S., Iyetomi H., Ichimaru S. 1983, ApJ, 273, 774
 Komatsu E. *et al.*, 2008, arXiv:0803.0547
 Landré V., Prantzos N., Aguer P., 1990, A.&A, 240, 85
 Levine E. S., Schulz A. E., White M. J., 2002, ApJ, 577, 569
 Maccio’ A., Dutton A. A., van den Bosch F. C., 2008, MNRAS, submitted, arXiv:0805.1926
 Mapelli M., Ferrara A., 2005, MNRAS, 364, 2
 Marigo, P., Girardi, L., Chiosi C., Wood, P.R. 2001, A&A, 371, 152
 Marigo, P., Chiosi, C., Kudritzki, R.-P., 2003, A&A, 399, 617
 Moskalenko I. V., Wai L. L., 2007, ApJ, 659, L29
 Nakamura F., Umemura M., 2001, ApJ, 548, 19

- Navarro J. F., Frenk C. S., White S. D. M., 1996, *ApJ*, 462, 563
 Omukai K., Nishi R. 1998, *ApJ*, 508, 141
 Omukai K., 2000, *ApJ*, 534, 809
 Omukai K., Palla F., 2003, *ApJ*, 589, 677
 O'Shea B., Norman M. L., 2007, *ApJ*, 654, 66
 Percival W. J., Cole S., Eisenstein D. J., Nichol R.C., Peacock J. A., Pope A. C., Szalay A. S., 2007, *MNRAS*, 381, 1053
 Reed D. *et al.*, 2005, *MNRAS*, 357, 82
 Riess A. G. *et al.*, 2007, *ApJ*, 659, 98
 Ripamonti E., Haardt F., Ferrara A., Colpi M., 2002, *MNRAS*, 334, 401
 Ripamonti E., Mapelli M., Ferrara A., 2007, *MNRAS*, 374, 1067
 Ripamonti E., Mapelli M., Ferrara A., 2007, *MNRAS*, 375, 1399
 Rogers F. J., Iglesias C. A., 1992, *ApJS*, 79, 507
 Salati P., Silk J., 1989, *ApJS*, 338, 24
 Salvadori S., Schneider R., Ferrara A., 2007, *MNRAS*, 381, 647
 Schneider R., Ferrara A., Natarayan P., Omukai K., 2000, *ApJ*, 571, 30
 Schneider R., Guetta D., Ferrara A., 2002, *MNRAS*, 334, 173
 Schneider R., Salvaterra R., Ferrara A., Ciardi B. 2006, *MNRAS*, 369, 825
 Scott P., Edsjo J., Fairbairn M., arXiv:0711.0991 [astro-ph]
 Spergel D. N. *et al.* 2007, *ApJS*, 170, 377
 Spolyar D., Freese K., Gondolo P., 2008, *Phys. Rev. Lett.*, 100, 051101
 Straniero O., 1988, *A.&A.*, 76, 157
 Tan J. C., McKee C., 2004, *ApJ*, 603, 383
 Tornatore L., Ferrara A., Schneider R., 2007, *MNRAS*, 382, 945
 Tumlinson J., 2006, *ApJ*, 641, 1
 Turk M. J., 2008, in "First Stars III", AIP Conf. Proc., 990, T. Abel, A. Heger, and B. W. O. Shea eds
 Yoshida N., Omukai K., Hernquist L., Abel T., 2006, *ApJ*, 652, 6
 Yoshida N., Omukai K., Hernquist L., 2007, *ApJ*, 667, L117
 Young P., 1980, *ApJ*, 242, 1932

APPENDIX A: STELLAR EVOLUTION

A1 The code

The modifications introduced in the Padova stellar code to follow the evolution of zero-metallicity stars are fully described in Marigo *et al.* (2001, 2003) to which the reader is referred for details.

In the following we summarize the main input physics and further implementation required to follow the pre-main sequence phase.

Radiative opacities are from the OPAL group, Rogers & Iglesias (1992) and Iglesias & Rogers (1993), for temperatures $T \geq 10^4$ K, and from Alexander & Ferguson (1994) for $T < 10^4$ K. Conductive opacities of electron-degenerate matter are from Itoh *et al.* (1983).

The equation of state for temperatures higher than 10^7 K is that of a fully-ionized gas. At high densities, Coulomb interactions are introduced adopting the prescription by Straniero (1988)

Nuclear reaction rates are from the compilation of Caughlan & Fowler (1988) while, energy losses by pair, plasma, and bremsstrahlung neutrinos, are from Haft, Raffelt & Weiss (1995).

The energy transport in the outer convection zone is described according to the mixing-length theory of Böhm-Vitense (1958) with a mixing length parameter, $\alpha = 1.68$, obtained from the calibration of the solar model by Girardi *et al.* (2000).

The extension of convective boundaries is estimated with the standard Schwarzschild criterion. Adopting more sophisticated schemes such as semiconvection and/or convective overshoot (e.g. Bressan *et al.* 1981 and Alongi *et al.* 1991) would not change the results.

Effects of stellar rotation and/or magnetic fields have not been considered in this exploratory work.

We finally remark that for zero-metallicity stars the abundance equations need to be solved simultaneously, for both the H and He burning reactions without any assumption for nuclear equilibria. This is performed with a semi-implicit extrapolation scheme (Bader & Deuffhard 1983).

A2 Evolutionary Tracks

We have computed evolutionary tracks for initial masses in the range $5 M_{\odot}$ to $600 M_{\odot}$, starting from the pre-main sequence phase and covering the central Hydrogen and Helium burning phases. The adopted initial composition consists of a mixture of just hydrogen and helium, resembling the lack of metals in the early Universe (Iocco *et al.* 2007), with mass fractions of $X = 0.755$ and $Y = 0.245$, respectively.

The evolution is performed at constant mass, i.e. neglecting both mass accretion during the pre-main sequence phase and mass loss by stellar winds in the later stages.

Five different sets of tracks have been considered, depending on the assumptions concerning the DM parameters. The results are summarized in Tables A1 to A5. For selected stages during the evolution we report: age, surface luminosity L , effective temperature T_{eff} , radius R_* , central values of density ρ_c , temperature T_c and hydrogen fraction X_c , and the fractional luminosity provided by nuclear reactions (L_{Nuc}/L_*).

Table A1 refers to stellar evolution without DM effects (the standard case). In Table A2 we consider only the effects of annihilation of DM in the adiabatic contraction phase. Tracks in tables A3 and A4 also take into account the additional role of DM scattering/capture processes for two different values of the parameter σ_0 , $\sigma_0 = 10^{-39} \text{cm}^2$ and $\sigma_0 = 10^{-38} \text{cm}^2$. Finally in Table A5 we have analysed the influence of a different neutralino mass (200 GeV instead of 100 GeV) on the adiabatic contraction phase.

The different stages selected in the Tables have the following meaning.

The *Starting Point* marks the beginning of the evolutionary sequences. In the standard case this is the first point where the model is fully and consistently supported by the gravitational energy release, while in the AC cases it is the model where the total luminosity of the star is equalized by the AC luminosity of its current baryonic configuration. At these luminosities the contraction timescale are of the order of a few years, so that some differences in the starting luminosity do not affect the subsequent evolutionary timescales.

The *Hayashi Minimum Luminosity Model* corresponds to the stage of minimum luminosity during the descent along the Hayashi locus. Soon after this point the proto-star moves towards the main sequence at nearly constant luminosity. This is a convenient point for comparing the contraction timescales of the different sets and their sensitivity to DM adiabatic contraction.

The points labelled $L_{AC}/L_*=50\%$ and 10% indicate the stages when the AC luminosity contributes to the 50% and

10%, respectively, of the total stellar luminosity. The complementary energy source comes from gravitational contraction. When $L_{AC}/L_* = 10\%$, the adiabatic contraction phase is essentially over.

The stage $L_{Nuc.}/L_* = 95\%$ indicate the point where the nuclear energy source provides 95% of the stellar luminosity. In absence of DM scattering/capture this point indicates the beginning of the major Hydrogen nuclear burning phase. On the contrary when DM scattering/capture becomes efficient, this point may be reached at an advanced stage of nuclear burning, or even not reached at all, for stars that suffer SC stalling. The contribution of the SC energy source makes the nuclear burning to occur at a slower rate, thus prolonging the lifetime of the star by a significant amount. In some circumstances the star is practically totally sustained by the SC luminosity with a negligible nuclear burning. In all these cases we provide the central hydrogen fraction and the fractional nuclear luminosity. These quantities may help the reader to evaluate the importance of the effect and, for the stalled stars, to roughly estimate the duration of the phase.

Finally, the last stage in the tables corresponds either to central Hydrogen exhaustion, or to the stalled model at an age of 5 Myr. We remark that, in the latter case, the stellar tracks have been evolved for a much longer time (larger than the standard Hydrogen burning lifetime) to properly check the stalling condition. In Tables A3 and A4 we do not report the first stages because they are identical to those in Table A2.

A few remarks on the effects of the AC and SC mechanisms are worthy at this point.

The AC term is important in the early contraction pre-main sequence phase. By comparing AC and Standard models we notice that, while the absolute duration of this phase increases as the mass decreases, the relative effect (i.e. the ratio between lifetimes at the Hayashi Minimum for a given mass) increases strongly with the stellar mass. In any case the AC phase does not particularly affect the total nuclear burning lifetime. Actually some Standard models show slightly longer Hydrogen burning lifetimes compared to the corresponding AC cases. This reflects the fact that the beginning of the main sequence is reached with small structural differences (e.g. location of convective boundaries), that propagates during the subsequent evolution.

The SC term is never important in the pre-main sequence contraction phase since the large stellar radii strongly limit the SC luminosity (directly via Eq. (14) and indirectly through the corrective term due to thermalization time, Eq. (6)).

This paper has been typeset from a $\text{\TeX}/\text{\LaTeX}$ file prepared by the author.

Table A1. The values for “standard”, metal-free stars evolving without DM annihilation.

M/M _⊙	Age(Myrs)	Log(L/L _⊙)	Log(T _{eff})	R _* (cm)	Log(ρ _c)	Log(T _c)	X _c	L _{Nuc} /L _*
Starting Point								
5	0.0000000	4.762	3.646	2.8556 10 ¹³	-6.317	4.898	-	-
7	0.0000000	4.854	3.651	3.0992 10 ¹³	-6.269	5.008	-	-
9	0.0000000	5.096	3.649	4.1400 10 ¹³	-6.611	4.962	-	-
12	0.0000000	5.223	3.652	4.7252 10 ¹³	-6.650	5.014	-	-
15	0.0000000	5.305	3.656	5.0942 10 ¹³	-6.624	5.068	-	-
20	0.0000000	5.416	3.660	5.6816 10 ¹³	-6.604	5.129	-	-
40	0.0000000	5.769	3.669	8.1776 10 ¹³	-6.692	5.211	-	-
100	0.0000000	6.178	3.699	1.1439 10 ¹⁴	-6.543	5.377	-	-
200	0.0000000	6.471	3.715	1.4849 10 ¹⁴	-6.495	5.466	-	-
400	0.0000000	6.782	3.736	1.9334 10 ¹⁴	-6.449	5.547	-	-
600	0.0000000	7.001	3.749	2.3371 10 ¹⁴	-6.471	5.575	-	-
Hayashi Minimum Luminosity Model								
5	0.0180837	2.643	3.739	1.6218 10 ¹²	-2.038	6.237	-	-
7	0.0069470	3.103	3.730	2.8721 10 ¹²	-2.640	6.129	-	-
9	0.0035714	3.432	3.724	4.3114 10 ¹²	-3.058	6.058	-	-
12	0.0016542	3.790	3.717	6.7326 10 ¹²	-3.558	5.971	-	-
15	0.0010506	4.057	3.713	9.3245 10 ¹²	-3.838	5.931	-	-
20	0.0005610	4.375	3.708	1.3782 10 ¹³	-4.261	5.861	-	-
40	0.0002053	5.034	3.703	3.0049 10 ¹³	-4.917	5.776	-	-
100	0.0000618	5.742	3.707	6.6582 10 ¹³	-5.633	5.672	-	-
200	0.0000261	6.265	3.726	1.1135 10 ¹⁴	-5.990	5.632	-	-
400	0.0000132	6.748	3.754	1.7054 10 ¹⁴	-6.154	5.644	-	-
600	0.0000039	6.997	3.757	2.2503 10 ¹⁴	-6.372	5.608	-	-
L _{Nuc} /L _* = 95%								
5	0.7510101	2.925	4.453	8.3722 10 ¹⁰	2.090	7.676	0.75194	9.5000 10 ⁻¹
7	0.4728800	3.378	4.552	8.9459 10 ¹⁰	2.114	7.777	0.75154	9.5001 10 ⁻¹
9	0.3380348	3.705	4.624	9.3718 10 ¹⁰	2.139	7.851	0.75111	9.5000 10 ⁻¹
12	0.2012758	4.072	4.703	9.9462 10 ¹⁰	2.169	7.931	0.75197	9.5000 10 ⁻¹
15	0.1537508	4.340	4.762	1.0292 10 ¹¹	2.200	7.992	0.75210	9.5000 10 ⁻¹
20	0.1005507	4.699	4.829	1.1443 10 ¹¹	2.201	8.051	0.75305	9.5000 10 ⁻¹
40	0.0407115	5.456	4.921	1.7910 10 ¹¹	1.998	8.100	0.75440	9.5001 10 ⁻¹
100	0.0220905	6.161	4.988	2.9595 10 ¹¹	1.748	8.138	0.75480	9.5002 10 ⁻¹
200	0.0167265	6.599	5.018	4.2737 10 ¹¹	1.585	8.159	0.75480	9.5224 10 ⁻¹
400	0.0136819	6.995	5.033	6.2788 10 ¹¹	1.443	8.177	0.75490	9.5000 10 ⁻¹
600	0.0130140	7.208	5.039	7.8188 10 ¹¹	1.359	8.185	0.75490	9.5001 10 ⁻¹
Central Hydrogen= 0								
5	55.5662916	3.336	4.504	1.0655 10 ¹¹	3.214	7.974	0.00000	0.0000
7	29.3981445	3.728	4.567	1.2473 10 ¹¹	2.916	8.039	0.00000	0.0000
9	19.8050932	4.061	4.602	1.5618 10 ¹¹	2.758	8.077	0.00000	0.0000
12	14.0895636	4.456	4.638	2.0846 10 ¹¹	2.604	8.110	0.00000	0.0000
15	10.5241264	4.716	4.666	2.4681 10 ¹¹	2.520	8.129	0.00000	0.0000
20	7.6663778	5.034	4.695	3.1161 10 ¹¹	2.411	8.150	0.00000	0.0000
40	4.1366357	5.666	4.740	5.2562 10 ¹¹	2.216	8.188	0.00000	0.0000
100	2.6233011	6.311	4.748	1.0603 10 ¹²	1.981	8.219	0.00000	0.0000
200	2.1888969	6.718	4.736	1.7944 10 ¹²	1.824	8.236	0.00000	0.0000
400	1.9639194	7.088	4.659	3.9227 10 ¹²	1.693	8.254	0.00000	0.0000
600	2.0630663	7.418	4.785	3.2025 10 ¹²	1.594	8.268	0.00000	0.0000

Table A2. AC mechanism only

M/M _⊙	Age(Myrs)	Log(L/L _⊙)	Log(T _{eff})	R _* (cm)	Log(ρ _c)	Log(T _c)	X _c	L _{Nuc} /L _*
Starting Point								
5	0.0000000	5.022	3.637	4.0174 10 ¹³	-6.924	4.712	-	-
7	0.0000000	5.151	3.642	4.5638 10 ¹³	-6.930	4.798	-	-
9	0.0000000	5.247	3.645	5.0209 10 ¹³	-6.943	4.860	-	-
12	0.0000000	5.357	3.648	5.6097 10 ¹³	-6.945	4.922	-	-
15	0.0000000	5.444	3.651	6.1288 10 ¹³	-6.941	4.968	-	-
20	0.0000000	5.556	3.655	6.8376 10 ¹³	-6.919	5.027	-	-
40	0.0000000	5.837	3.667	8.9564 10 ¹³	-6.845	5.161	-	-
100	0.0000000	6.257	3.699	1.2491 10 ¹⁴	-6.670	5.334	-	-
200	0.0000000	6.547	3.715	1.6202 10 ¹⁴	-6.622	5.424	-	-
400	0.0000000	6.844	3.733	2.0996 10 ¹⁴	-6.576	5.504	-	-
600	0.0000000	7.021	3.747	2.4173 10 ¹⁴	-6.533	5.555	-	-
L _{AC} /L _* =50%								
5	0.0096533	3.074	3.717	2.9553 10 ¹²	-3.216	5.937	-	-
7	0.0151310	3.201	3.722	3.3305 10 ¹²	-3.086	6.018	-	-
9	0.0177185	3.449	3.724	4.3954 10 ¹²	-3.043	6.067	-	-
12	0.0175911	3.886	3.726	7.2124 10 ¹²	-3.174	6.095	-	-
15	0.0163967	4.187	3.728	1.0079 10 ¹³	-3.375	6.086	-	-
20	0.0144465	4.546	3.748	1.3908 10 ¹³	-3.608	6.081	-	-
40	0.0092501	5.259	3.766	2.9110 10 ¹³	-4.295	5.992	-	-
100	0.0053198	6.040	3.943	3.1780 10 ¹³	-4.055	6.204	-	-
200	0.0036779	6.514	4.041	3.4862 10 ¹³	-3.914	6.326	-	-
400	0.0024905	6.935	4.094	4.4213 10 ¹³	-3.871	6.406	-	-
600	0.0020670	7.164	4.110	5.3619 10 ¹³	-3.881	6.439	-	-
L _{AC} /L _* =10%								
5	0.0518843	2.801	3.763	1.7432 10 ¹²	-1.456	6.419	-	-
7	0.0419409	3.354	3.891	1.8255 10 ¹²	-1.346	6.559	-	-
9	0.0341297	3.719	3.969	1.9446 10 ¹²	-1.371	6.623	-	-
12	0.0287672	4.110	4.070	1.9156 10 ¹²	-1.305	6.726	-	-
15	0.0250591	4.388	4.134	1.9676 10 ¹²	-1.293	6.788	-	-
20	0.0215014	4.719	4.221	1.9227 10 ¹²	-1.205	6.888	-	-
40	0.0136990	5.392	4.365	2.1521 10 ¹²	-1.184	7.036	-	-
100	0.0076639	6.099	4.454	3.2231 10 ¹²	-1.376	7.098	-	-
200	0.0057030	6.553	4.527	3.8831 10 ¹²	-1.310	7.194	-	-
400	0.0042986	6.959	4.571	5.0526 10 ¹²	-1.316	7.258	-	-
600	0.0037723	7.180	4.586	6.0964 10 ¹²	-1.352	7.281	-	-
Hayashi Minimum Luminosity Model								
5	0.0318454	2.650	3.739	1.6363 10 ¹²	-2.062	6.232	-	-
7	0.0207489	3.115	3.730	2.9142 10 ¹²	-2.650	6.130	-	-
9	0.0177888	3.449	3.724	4.3936 10 ¹²	-3.036	6.069	-	-
12	0.0153947	3.814	3.717	6.9172 10 ¹²	-3.536	5.982	-	-
15	0.0144330	4.089	3.713	9.6710 10 ¹²	-3.842	5.936	-	-
20	0.0124400	4.410	3.707	1.4378 10 ¹³	-4.283	5.859	-	-
40	0.0082365	5.094	3.699	3.2837 10 ¹³	-5.150	5.707	-	-
100	0.0043604	5.805	3.704	7.2797 10 ¹³	-5.820	5.613	-	-
200	0.0024627	6.297	3.721	1.1845 10 ¹⁴	-6.130	5.587	-	-
400	0.0009528	6.748	3.739	1.8375 10 ¹⁴	-6.366	5.574	-	-
600	0.0004468	6.998	3.756	2.2582 10 ¹⁴	-6.386	5.603	-	-
L _{Nuc} /L _* = 95%								
5	0.6821600	2.928	4.452	8.4617 10 ¹⁰	2.079	7.672	0.75305	9.5000 10 ⁻¹
7	0.4372555	3.380	4.551	9.0212 10 ¹⁰	2.105	7.774	0.75265	9.5000 10 ⁻¹
9	0.3242375	3.707	4.623	9.4319 10 ¹⁰	2.133	7.849	0.75211	9.5000 10 ⁻¹
12	0.2193152	4.071	4.703	9.9367 10 ¹⁰	2.169	7.931	0.75208	9.5000 10 ⁻¹
15	0.1737158	4.342	4.762	1.0320 10 ¹¹	2.198	7.992	0.75206	9.5000 10 ⁻¹
20	0.1152623	4.699	4.829	1.1440 10 ¹¹	2.201	8.051	0.75310	9.5000 10 ⁻¹
40	0.0510427	5.455	4.921	1.7890 10 ¹¹	1.999	8.100	0.75440	9.5001 10 ⁻¹
100	0.0278809	6.161	4.988	2.9578 10 ¹¹	1.749	8.138	0.75480	9.5001 10 ⁻¹
200	0.0208053	6.599	5.018	4.2722 10 ¹¹	1.586	8.159	0.75480	9.5001 10 ⁻¹
400	0.0168216	6.995	5.033	6.2819 10 ¹¹	1.442	8.177	0.75490	9.5001 10 ⁻¹
600	0.0152766	7.208	5.039	7.8170 10 ¹¹	1.360	8.185	0.75490	9.5080 10 ⁻¹
Central Hydrogen= 0 or Scattering Stallation model								
5	56.1465439	3.340	4.505	1.0660 10 ¹¹	3.196	7.983	0.00000	0.0000
7	29.1142533	3.725	4.569	1.2323 10 ¹¹	2.929	8.037	0.00000	0.0000
9	19.2892971	4.046	4.607	1.4988 10 ¹¹	2.772	8.074	0.00000	0.0000
12	13.2154438	4.420	4.646	1.9311 10 ¹¹	2.624	8.107	0.00000	0.0000
15	10.7956074	4.734	4.663	2.5626 10 ¹¹	2.515	8.131	0.00000	0.0000
20	7.6619203	5.035	4.695	3.1251 10 ¹¹	2.415	8.151	0.00000	0.0000
40	4.1429360	5.667	4.740	5.2378 10 ¹¹	2.219	8.189	0.00000	0.0000
100	2.6907600	6.325	4.740	1.1194 10 ¹²	1.986	8.222	0.00000	0.0000
200	2.1910250	6.720	4.712	2.0064 10 ¹²	1.831	8.239	0.00000	0.0000
400	2.2893942	7.330	5.117	6.2717 10 ¹¹	1.663	8.269	0.00000	0.0000
600	1.8355234	7.289	4.543	8.4022 10 ¹²	1.612	8.261	0.00000	0.0000

Table A3. AC and SC mechanisms active; $\rho_\chi = 10^{11} \text{GeV}/\text{cm}^3$, $\sigma_0 = 10^{-39} \text{cm}^2$

M/M $_{\odot}$	Age(Myrs)	Log(L/L $_{\odot}$)	Log(T $_{eff}$)	R*(cm)	Log(ρ_c)	Log(T $_c$)	X $_c$	L $_{Nuc}$ /L*
Hayashi Minimum Luminosity Model								
5	0.0321649	2.650	3.739	1.6353 10 ¹²	-2.056	6.233	-	-
7	0.0207489	3.115	3.730	2.9142 10 ¹²	-2.650	6.130	-	-
9	0.0177888	3.449	3.724	4.3936 10 ¹²	-3.036	6.069	-	-
12	0.0153947	3.814	3.717	6.9172 10 ¹²	-3.536	5.982	-	-
15	0.0144330	4.089	3.713	9.6710 10 ¹²	-3.842	5.936	-	-
20	0.0124400	4.410	3.707	1.4378 10 ¹³	-4.283	5.859	-	-
40	0.0082365	5.094	3.699	3.2837 10 ¹³	-5.150	5.707	-	-
100	0.0043604	5.805	3.704	7.2797 10 ¹³	-5.820	5.613	-	-
200	0.0024627	6.297	3.721	1.1845 10 ¹⁴	-6.130	5.587	-	-
300	0.0016023	6.565	3.732	1.5320 10 ¹⁴	-6.254	5.585	-	-
400	0.0009528	6.748	3.739	1.8375 10 ¹⁴	-6.366	5.574	-	-
600	0.0004468	6.998	3.756	2.2582 10 ¹⁴	-6.386	5.603	-	-
L $_{Nuc}$ /L* = 95%								
7	58.2469694	3.692	4.559	1.2448 10 ¹¹	2.532	7.974	0.11475	9.5000 10 ⁻¹
9	30.9662677	3.992	4.607	1.4085 10 ¹¹	2.378	7.985	0.15375	9.5000 10 ⁻¹
12	15.8442989	4.330	4.663	1.6080 10 ¹¹	2.226	7.997	0.21329	9.5000 10 ⁻¹
15	10.3999383	4.586	4.707	1.7632 10 ¹¹	2.117	8.006	0.27733	9.5000 10 ⁻¹
20	6.3947664	4.879	4.758	1.9554 10 ¹¹	2.001	8.018	0.34013	9.5000 10 ⁻¹
40	2.4225710	5.507	4.856	2.5643 10 ¹¹	1.767	8.043	0.46558	9.5000 10 ⁻¹
100	1.1063569	6.203	4.935	3.9656 10 ¹¹	1.529	8.075	0.57258	9.5179 10 ⁻¹
200	0.9510749	6.633	4.950	6.0802 10 ¹¹	1.356	8.089	0.53188	9.4999 10 ⁻¹
300	0.9983394	6.866	4.946	8.1006 10 ¹¹	1.263	8.096	0.48495	9.4997 10 ⁻¹
400	1.1107156	7.027	4.933	1.0328 10 ¹²	1.200	8.101	0.42339	9.5000 10 ⁻¹
600	0.9687933	7.246	4.963	1.1603 10 ¹²	1.121	8.109	0.45154	9.4998 10 ⁻¹
Central Hydrogen= 0 or Scattering Stallation model								
5 ^s	5.0000000	2.830	4.322	1.3769 10 ¹¹	1.384	7.452	0.75400	4.8940 10 ⁻²
7	60.2205803	3.758	4.563	1.3173 10 ¹¹	2.903	8.048	0.00000	0.0000
9	32.9417891	4.076	4.603	1.5812 10 ¹¹	2.758	8.079	0.00000	0.0000
12	17.9675788	4.441	4.642	2.0086 10 ¹¹	2.615	8.109	0.00000	0.0000
15	12.6592264	4.728	4.665	2.5143 10 ¹¹	2.517	8.131	0.00000	0.0000
20	8.6058962	5.038	4.695	3.1378 10 ¹¹	2.414	8.151	0.00000	0.0000
40	4.3902484	5.670	4.740	5.2772 10 ¹¹	2.218	8.190	0.00000	0.0000
100	2.9876710	6.358	4.609	2.1264 10 ¹²	1.978	8.225	0.00000	0.0000
200	2.3571500	6.730	4.639	2.8487 10 ¹²	1.834	8.240	0.00000	0.0000
300	2.1357779	6.942	4.651	3.4292 10 ¹²	1.747	8.248	0.00000	0.0000
400	2.0465587	7.106	4.637	4.4207 10 ¹²	1.691	8.255	0.00000	0.0000
600	2.0407706	7.362	4.810	2.6816 10 ¹²	1.595	8.265	0.00000	0.0000

^s Track Stalled

Table A4. AC and SC mechanisms active; $\rho_\chi = 10^{11} \text{GeV}/\text{cm}^3$, $\sigma_0 = 10^{-38} \text{cm}^2$

M/M $_{\odot}$	Age(Myrs)	Log(L/L $_{\odot}$)	Log(T $_{eff}$)	R*(cm)	Log(ρ_c)	Log(T $_c$)	X $_c$	L $_{Nuc}$ /L*
Hayashi Minimum Luminosity Model								
5	0.0732837	2.865	3.859	1.2047 10 ¹²	-0.975	6.618	-	-
7	0.0207489	3.115	3.730	2.9142 10 ¹²	-2.650	6.130	-	-
9	0.0177888	3.449	3.724	4.3936 10 ¹²	-3.036	6.069	-	-
12	0.0153947	3.814	3.717	6.9172 10 ¹²	-3.536	5.982	-	-
15	0.0144330	4.089	3.713	9.6710 10 ¹²	-3.842	5.936	-	-
20	0.0124400	4.410	3.707	1.4378 10 ¹³	-4.283	5.859	-	-
40	0.0082365	5.094	3.699	3.2837 10 ¹³	-5.150	5.707	-	-
100	0.0043604	5.805	3.704	7.2797 10 ¹³	-5.820	5.613	-	-
200	0.0030809	6.284	3.723	1.1551 10 ¹⁴	-6.077	5.605	-	-
400	0.0016042	6.745	3.748	1.7519 10 ¹⁴	-6.234	5.618	-	-
600	0.0004468	6.998	3.756	2.2582 10 ¹⁴	-6.386	5.603	-	-
L $_{Nuc}$ /L* = 95%								
40	20.7324568	5.628	4.754	4.7132 10 ¹¹	1.800	8.058	0.10605	9.5000 10 ⁻¹
100	4.5980377	6.279	4.792	8.3431 10 ¹¹	1.540	8.080	0.12656	9.5133 10 ⁻¹
200	3.5912405	6.718	4.748	1.7011 10 ¹²	1.375	8.094	0.14434	9.5000 10 ⁻¹
400	3.4325657	7.085	4.740	2.6877 10 ¹²	1.241	8.110	0.11646	9.4998 10 ⁻¹
600	3.9629294	7.308	4.652	5.2214 10 ¹²	1.185	8.122	0.08405	9.5000 10 ⁻¹
Central Hydrogen= 0 or Scattering Stallation model								
5 ^s	5.0000000	2.698	3.732	1.7904 10 ¹²	-2.567	6.154	0.75500	0.0000
7 ^s	5.0000000	3.191	3.956	1.1241 10 ¹²	-1.067	6.721	0.75500	1.5187 10 ⁻⁸
9 ^s	5.0000000	3.578	4.119	8.2850 10 ¹¹	-0.652	6.925	0.75500	3.4554 10 ⁻⁷
12 ^s	5.0000000	3.984	4.309	5.5088 10 ¹¹	-0.068	7.190	0.75500	1.6556 10 ⁻⁵
15 ^s	5.0000000	4.274	4.438	4.2336 10 ¹¹	0.342	7.376	0.75500	2.6014 10 ⁻⁴
20 ^s	5.0000000	4.630	4.581	3.3130 10 ¹¹	0.774	7.578	0.75440	2.2035 10 ⁻³
40	21.0633259	5.674	4.735	5.4184 10 ¹¹	2.218	8.190	0.00000	0.0000
100	4.8774489	6.311	4.749	1.0565 10 ¹²	1.984	8.220	0.00000	0.0000
200	3.8658341	6.744	4.619	3.1638 10 ¹²	1.833	8.241	0.00000	0.0000
400	3.6641729	7.105	4.454	1.0244 10 ¹³	1.702	8.256	0.00000	0.0000
600	4.1027411	7.322	4.418	1.5577 10 ¹³	1.626	8.265	0.00000	0.0000

^s Track Stalled

Table A5. AC mechanism only, for a neutralino mass $m_{\chi}=200\text{GeV}$.

M/M _⊙	Age(Myrs)	Log(L/L _⊙)	Log(T _{eff})	R _* (cm)	Log(ρ _c)	Log(T _c)	X _c	L _{Nuc} /L _*
Starting Point								
5	0.0000000	4.882	3.642	3.3438 10 ¹³	-6.576	4.810	-	-
7	0.0000000	5.009	3.647	3.7899 10 ¹³	-6.601	4.901	-	-
9	0.0000000	5.104	3.649	4.1733 10 ¹³	-6.615	4.960	-	-
12	0.0000000	5.212	3.653	4.6489 10 ¹³	-6.615	5.025	-	-
15	0.0000000	5.236	3.659	4.6423 10 ¹³	-6.465	5.119	-	-
20	0.0000000	5.417	3.660	5.6860 10 ¹³	-6.603	5.129	-	-
40	0.0000000	5.699	3.673	7.4259 10 ¹³	-6.532	5.264	-	-
100	0.0000000	6.099	3.698	1.0491 10 ¹⁴	-6.421	5.417	-	-
200	0.0000000	6.400	3.716	1.3640 10 ¹⁴	-6.370	5.508	-	-
400	0.0000000	6.763	3.752	1.7578 10 ¹⁴	-6.187	5.633	-	-
600	0.0000000	7.030	3.786	2.0377 10 ¹⁴	-6.004	5.730	-	-
L _{AC} /L _* =50%								
5	0.0080226	3.090	3.716	3.0198 10 ¹²	-3.244	5.928	-	-
7	0.0123634	3.216	3.722	3.3996 10 ¹²	-3.128	6.007	-	-
9	0.0139301	3.452	3.723	4.4418 10 ¹²	-3.139	6.040	-	-
12	0.0140096	3.872	3.724	7.1618 10 ¹²	-3.235	6.074	-	-
15	0.0116689	4.174	3.724	1.0123 10 ¹³	-3.451	6.060	-	-
20	0.0108273	4.537	3.738	1.4423 10 ¹³	-3.669	6.059	-	-
40	0.0070071	5.266	3.778	2.7769 10 ¹³	-4.223	6.017	-	-
100	0.0039907	6.043	3.975	2.7385 10 ¹³	-3.902	6.255	-	-
200	0.0025829	6.516	4.059	3.2085 10 ¹³	-3.826	6.355	-	-
400	0.0016259	6.935	4.111	4.0936 10 ¹³	-3.796	6.431	-	-
600	0.0013353	7.164	4.129	4.9076 10 ¹³	-3.795	6.467	-	-
L _{AC} /L _* =10%								
5	0.0509513	2.806	3.765	1.7354 10 ¹²	-1.431	6.428	-	-
7	0.0406938	3.361	3.907	1.7131 10 ¹²	-1.271	6.585	-	-
9	0.0315087	3.723	3.980	1.8568 10 ¹²	-1.318	6.642	-	-
12	0.0257831	4.113	4.081	1.8228 10 ¹²	-1.248	6.745	-	-
15	0.0207747	4.390	4.144	1.8789 10 ¹²	-1.240	6.806	-	-
20	0.0182315	4.720	4.235	1.8072 10 ¹²	-1.131	6.912	-	-
40	0.0115195	5.392	4.374	2.0643 10 ¹²	-1.133	7.053	-	-
100	0.0063115	6.100	4.458	3.1661 10 ¹²	-1.354	7.105	-	-
200	0.0044895	6.553	4.521	3.9951 10 ¹²	-1.346	7.182	-	-
400	0.0032827	6.958	4.559	5.3438 10 ¹²	-1.387	7.234	-	-
600	0.0029023	7.180	4.574	6.4304 10 ¹²	-1.418	7.259	-	-
Hayashi Minimum Luminosity Model								
5	0.0300699	2.650	3.739	1.6362 10 ¹²	-2.059	6.233	-	-
7	0.0182169	3.115	3.730	2.9145 10 ¹²	-2.650	6.130	-	-
9	0.0148365	3.449	3.724	4.3933 10 ¹²	-3.037	6.068	-	-
12	0.0122626	3.814	3.717	6.9151 10 ¹²	-3.539	5.981	-	-
15	0.0101071	4.088	3.713	9.6724 10 ¹²	-3.855	5.932	-	-
20	0.0091717	4.409	3.707	1.4361 10 ¹³	-4.275	5.861	-	-
40	0.0061004	5.091	3.700	3.2531 10 ¹³	-5.074	5.731	-	-
100	0.0026849	5.807	3.703	7.3077 10 ¹³	-5.838	5.608	-	-
200	0.0009983	6.297	3.721	1.1832 10 ¹⁴	-6.124	5.589	-	-
400	0.0000092	6.761	3.752	1.7546 10 ¹⁴	-6.186	5.634	-	-
600	0.0000092	7.029	3.786	2.0349 10 ¹⁴	-6.002	5.730	-	-
L _{Nuc} /L _* = 95%								
5	0.6992481	2.927	4.452	8.4513 10 ¹⁰	2.080	7.673	0.75283	9.5000 10 ⁻¹
7	0.4522332	3.380	4.551	8.9905 10 ¹⁰	2.108	7.775	0.75226	9.5000 10 ⁻¹
9	0.3378005	3.705	4.623	9.3935 10 ¹⁰	2.137	7.850	0.75159	9.5000 10 ⁻¹
12	0.2151746	4.071	4.703	9.9326 10 ¹⁰	2.170	7.931	0.75200	9.5000 10 ⁻¹
15	0.1683067	4.342	4.762	1.0317 10 ¹¹	2.199	7.992	0.75207	9.5000 10 ⁻¹
20	0.1110554	4.699	4.829	1.1438 10 ¹¹	2.201	8.051	0.75310	9.5000 10 ⁻¹
40	0.0483624	5.455	4.921	1.7885 10 ¹¹	1.999	8.100	0.75440	9.5000 10 ⁻¹
100	0.0261951	6.161	4.988	2.9566 10 ¹¹	1.749	8.139	0.75480	9.5002 10 ⁻¹
200	0.0193638	6.599	5.018	4.2712 10 ¹¹	1.586	8.159	0.75480	9.5003 10 ⁻¹
400	0.0156433	6.994	5.033	6.2776 10 ¹¹	1.443	8.177	0.75490	9.6414 10 ⁻¹
600	0.0142502	7.208	5.039	7.8114 10 ¹¹	1.361	8.186	0.75490	9.6439 10 ⁻¹
Central Hydrogen= 0 or Scattering Stallation model								
5	56.1384003	3.340	4.505	1.0644 10 ¹¹	3.200	7.983	0.00000	0.0000
7	29.7313755	3.734	4.566	1.2641 10 ¹¹	2.924	8.040	0.00000	0.0000
9	19.5580299	4.053	4.604	1.5289 10 ¹¹	2.771	8.076	0.00000	0.0000
12	13.7294256	4.447	4.640	2.0425 10 ¹¹	2.613	8.110	0.00000	0.0000
15	10.7102756	4.726	4.665	2.5130 10 ¹¹	2.518	8.131	0.00000	0.0000
20	7.6979362	5.040	4.694	3.1552 10 ¹¹	2.415	8.152	0.00000	0.0000
40	4.1505195	5.668	4.741	5.2413 10 ¹¹	2.222	8.190	0.00000	0.0000
100	2.7010537	6.327	4.735	1.1476 10 ¹²	1.982	8.221	0.00000	0.0000
200	2.2941418	6.744	4.547	4.4148 10 ¹²	1.843	8.242	0.00000	0.0000
400 ^a	1.9648883	7.194	4.342	1.9067 10 ¹³	1.191	8.105	0.16920	9.7490 10 ⁻¹
600	2.0679154	7.538	5.111	8.2005 10 ¹¹	1.583	8.275	0.00000	0.0000

^a Problems to reach end of H-burning